ACS APPLIED MATERIALS & INTERFACES

Research Article

www.acsami.org

Scaling Up Nature: Large Area Flexible Biomimetic Surfaces

Yinyong Li,[†] Jacob John,[†] Kristopher W. Kolewe,[‡] Jessica D. Schiffman,[‡] and Kenneth R. Carter*[,†]

[†]Department of Polymer Science and Engineering, [‡]Department of Chemical Engineering, University of Massachusetts, Amherst, Massachusetts 01003, United States

Supporting Information

ABSTRACT: The fabrication and advanced function of large area biomimetic superhydrophobic surfaces (SHS) and slippery lubricant-infused porous surfaces (SLIPS) are reported. The use of roll-to-roll nanoimprinting techniques enabled the continuous fabrication of SHS and SLIPS based on hierarchically wrinkled surfaces. Perfluoropolyether hybrid molds were used as flexible molds for roll-to-roll imprinting into a newly designed thiol−ene based photopolymer resin coated on flexible polyethylene terephthalate films. The patterned surfaces exhibit feasible superhydrophobicity with a water contact angle around 160° without any further surface modification. The SHS can be easily converted into SLIPS by roll-to-roll coating of a fluorinated lubricant, and these surfaces have outstanding repellence to a variety of liquids. Furthermore, both SHS and SLIPS display antibiofouling properties when challenged with *Escherichia coli* K12 MG1655. The current article describes the transformation of artificial biomimetic structures from small, lab-scale coupons to low-cost, large area platforms.

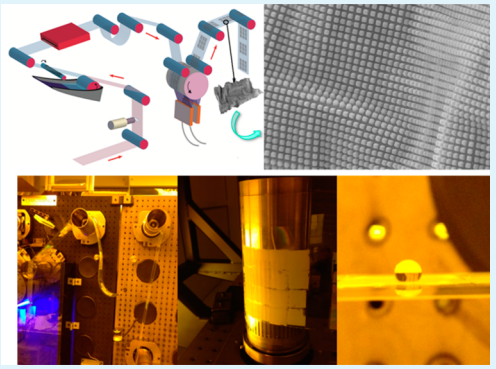

KEYWORDS: *nanoimprint, biomimetics, superhydrophobic, wrinkle, SLIPS, low cost*

INTRODUCTION

Nature presents fascinating examples of self-cleaning surfaces, such as rose petals, lotus leaves, water striders, and butterfly wings, which have inspired researchers to mimic their function. A commonly found self-cleaning surface is a lotus leaf-type superhydrophobic surface (SHS). Many efforts have been made to create a SHS, including layer-by-layer assembly,[1] phase separation,[2] nanoparticle composite coating,[3] sol−gel process,[4] electrospinning,[5] soft lithography,[6] and liquid flame spray.[7]

Alternatively, a different concept has been proposed to create self-cleaning surfaces. Inspired by *Nepenthes* pitcher plants, which retain lubricating liquid in hierarchical textures and form a slippery surface, Wong et al. developed a slippery liquid-infused porous surface (SLIPS), repellent to various liquids.[8] Such self-cleaning surfaces have great potential for fluid transportation, airplane and watercraft coatings, and medical applications because they exhibit low contact angle hysteresis, self-healing, anti-icing, and antibiofouling properties.[8−14]

To realize their full potential, self-cleaning surfaces need to be produced over a large area in a cost-efficient manner. Despite substantial attempts to achieve practical applications,[15,16] limitations still remain for the continuous and efficient fabrication of SHS, and few processes have been adopted by industry. This is due to most reported methods requiring multiple complex processing steps, harsh processing conditions, low throughput, substrate limitations, or high cost involved in their use.[17,18] Meanwhile, while research of SLIPS has emerged over the past few years, the continuous fabrication of SLIPS over large areas in a cost-effective manner has not yet been demonstrated. This gap may be attributed to difficulties in manufacturing large area substrates that have porous or patterned surfaces and chemical affinity to preserve the fluorinated lubricant. These criteria limit the choice of substrates to intrinsically porous materials with low surface energy, for instance, porous Teflon nanofibrous mats or prepatterned films that have been surface modified with low surface energy chemicals. These requirements, however, involve multiple tedious steps, including patterning, surface chemical treatment, and lubricant coating.[8] All of the restrictions mentioned have impeded the wider use of SHS and SLIPS.

Since Tan et al.[19] proposed roller nanoimprint lithography, it has been hailed as the most promising industrial technique for nanoimprint due to its high-throughput, low-cost, and ability to be a continuous process. Later, researchers from Guo's group developed a UV roll-to-roll nanoimprint lithography (R2R NIL) technique for high speed, continuous imprinting of sub-100 nm patterns on flexible substrates.[20,21] Recent development in R2R NIL[22] makes it a very promising technique for the fast and cheap fabrication of SHS and SLIPS for self-cleaning applications.

In the current study, we describe the fabrication and advanced function of biomimetic SHS and SLIPS. We sought to develop the ability to accomplish this rapidly over large areas using roll-to-roll nanoimprint lithography. By understanding the unique matching of new materials with new processes, a large area biomimetic SHS or SLIPS coating can be achieved

Received: June 5, 2015
Accepted: October 1, 2015
Published: October 1, 2015

DOI: 10.1021/acsami.5b04957
ACS Appl. Mater. Interfaces 2015, 7, 23439−23444

that presents extreme repellence to various liquids. To demonstrate the effectiveness of these biomimetic surfaces, their antibiofouling properties will be assessed.

EXPERIMENTAL SECTION

Materials. All reagents were used as received unless otherwise specified. 1,3,5-Triallyl-1,3,5-triazine-2,4,6(1*H*,3*H*,5*H*)-trione (TTT), pentaerythritol tetrakis(3-mercaptopropionate) (PETMP), propylene glycol monomethyl ether acetate (PGMEA), and benzoin methyl ether (BME) were purchased from Sigma-Aldrich. Perfluoropolyether acrylate (CN4002) was purchased from Sartomer USA, LLC. Norland Optical Adhesives 74 was purchased from Norland Products, NJ, USA. 1*H*,1*H*,2*H*,2*H*-Perfluorodecyl acrylate (PFDA) was purchased from Alfa Aesar, MA, USA. DuPont Krytox lubricant was purchased from Kurt J. Lesker company, USA. 2-Hydroxyethyl methacrylate (98%) was purchased from Acros Organics and poly(2-hydroxymethyl methacrylate) (PHEMA) was synthesized according to our previous work.[23]

Fabrication of Hierarchical Wrinkle Master Mold and Cross-Linked Perfluoropolyether Acrylate (PFPE) Hybrid Mold. The hierarchical wrinkle pattern was fabricated by inducing microsize wrinkles on prenanopatterned PHEMA films according to a method described previously.[24] Briefly, a hardened, cross-linked polydimethylsiloxane elastomer mold replicated from a master mold with pillar patterns (700 nm size, 1 μm periodicity, and 750 nm height) was imprinted into a PHEMA film. The nanopatterned PHEMA film was then immersed in a solution of toluene and methyltrichlorosilane (v/v, 100:5) at 100 °C and allowed to react to form wrinkling structures. The obtained hierarchical patterned surface with nanopillars and microwrinkles was treated with heptadecafluoro-1,1,2,2-tetrahydrodecyldimethylsilane and used as the master mold to replicate PFPE hybrid molds by UV NIL as the molds for the roll-to-roll process using a method described elsewhere.[25]

Preparation of UV-Curable Photoresist. A UV curable low surface energy photoresist based on thiol−ene chemistries was developed for R2R UV NIL. A small amount (ranging from 0.0 to 1.0 wt %) of PFDA was mixed with molar equivalent TTT and PETMP. BME (1.0 wt %) was added as a photoinitiator.

Roll-to-Roll (R2R) Nanoimprinting. Detailed procedures of R2R nanocoating and nanoimprinting have been described previously.[25] Briefly, PFPE hybrid molds were wrapped around the embossing roller using double-side tape. A coating solution consisting of 70 wt % photoresist in PGMEA was coated on a corona-treated PET web using a Mayer rod coating unit to achieve a ~5 μm thick resist film. The two vacuum rollers applied web tension against the photoresist-coated web and the molds when the web was fed into the embossing roller. The photoresist was cured using a UV light source (Omnicure 1000, EXFO), and the web with cured photoresist was continuously separated from molds and rewound on rewinding roller as the web moved forward. The web speed was kept at 10 in. min^{-1} for both coating and imprinting. Patterned web was then coated with a thin layer of DuPont Krytox lubricant using a Mayer rod coating unit to form SLIPS.

Evaluation of Bacteria Attachment. The antifouling properties of the samples were evaluated using *Escherichia coli* K12 MG1655 (*E. coli*), a similar strain as that used by Aizenberg et al.,[13] as model bacteria for attachment. Each sample was placed in a separate well of a 6-well polystyrene plate, to which 10 mL of M9 growth media containing ampicillin (100 μg mL^{-1}) was added. Overnight cultures of *E. coli* (1.0×10^8 cells mL^{-1}) grown in Difco Luria−Bertani broth with ampicillin (100 μg mL^{-1}) were inoculated into each well and incubated at 37 °C for 2 h. The growth media was then removed via a sterilized glass pipet, and the samples were lightly shaken and rinsed repeatedly three times with sterile phosphate buffered saline solution. The samples were then fixed for 10 min using fresh 4% paraformaldhyde, mounted between sterilized 22 mm glass coverslips, and sealed using an equal part mixture of Vaseline, lanoline, and paraffin wax (VALAP). To quantify the attachment of viable bacteria, confocal laser scanning microscopy (CLSM, Nikon-D Eclipse) with a 60× Nikon NF oil immersion objective and a green argon laser were used. Flat PET samples acted as an internal control to normalize the amount of bacteria that attached during each experiment. For each sample, 10−15 micrographs were randomly acquired with at least three parallel replicates. Subsequent image analysis was performed with ImageJ 1.45 software (National Institutes of Health, Bethesda, MD).

Characterization. Contact angles were measured using a VCA Optima surface analysis/goniometry system. Surface composition was analyzed by X-ray photoelectron spectroscopy using using a Physical Electronics Quantum 2000 Microprobe with monochromatic Al X-rays. Films surface structures characterization was carried out using an Olympus optical microscope, DI Dimension-3000 atomic force microscope, and JEOL JSM-7001F scanning electron microscope. Film thicknesses were analyzed using a Veeco Dektak Stylus Profilometer.

RESULTS AND DISCUSSION

To realize high-speed R2R UV NIL processes, resist materials should be stringently selected to satisfy several requirements: modest viscosity, good wetting properties, and fast curing speed with low shrinkage.[21] Photoresists based on the thiol−ene reaction of a multifunctional thiol monomer and a multifunctional ene compound are insensitive to oxygen inhibition and have fast curing rates with high conversion and low shrinkage,[26] making them suitable for fast R2R NIL with high feature fidelity. A thiol−ene based resist material consisting of 1,3,5-triallyl-1,3,5-triazine-2,4,6(1*H*,3*H*,5*H*)-trione (TTT) and pentaerythritol tetrakis(3-mercaptopropionate) (PETMP) has been successfully demonstrated for step and flash imprint lithography.[27] Moreover, surface chemistry and wetting behavior of this thiol−ene based coating can be controlled simply by incorporating numerous ene-containing comonomers with versatile functionalities into the resist. Hence, by utilizing an ultralow surface energy monomer, 1*H*,1*H*,2*H*,2*H*-perfluorodecyl acrylate (PFDA), a thiol−ene based hydrophobic resist was developed for fast R2R UV NIL (Figure 1).

The surface energy of resists containing varying PFDA content was approximated by Owens−Wendt analysis (eq 1)[28]

$$1 + \cos\theta = 2\sqrt{\gamma_{sv}^{d}}\left(\frac{\gamma_{lv}^{d}}{\gamma_{lv}}\right) + 2\sqrt{\gamma_{sv}^{h}}\left(\frac{\gamma_{lv}^{h}}{\gamma_{lv}}\right) \quad (1)$$

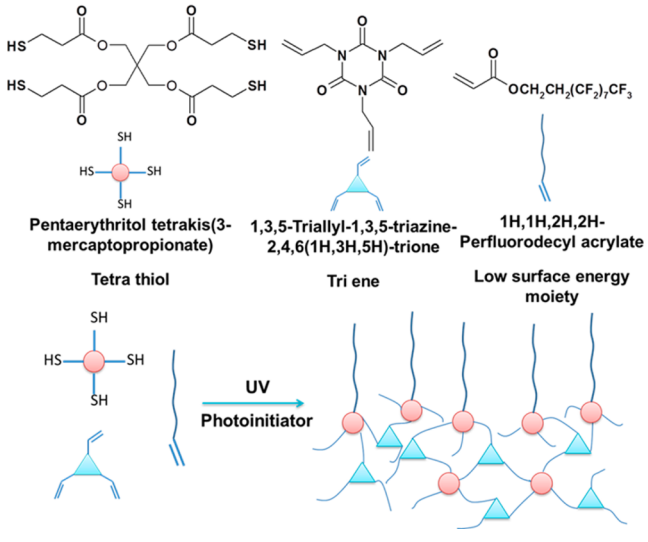

Figure 1. Thiol−ene based photoresist for R2R UV NIL.

DOI: 10.1021/acsami.5b04957
ACS Appl. Mater. Interfaces 2015, 7, 23439−23444

where θ is the liquid contact angle, γ_{lv} and γ_{sv} are the surface tension of liquid and solid, respectively, and superscripts h and d stand for polar (or hydrogen bonding) and dispersive components of surface tension.

Water (γ_{lv}^d = 21.8 mN m^{-1} and γ_{lv}^h = 51.0 mN m^{-1}) and hexadecane (γ_{lv}^d = 27.5 mN m^{-1} and γ_{lv}^h = 0.0 mN m^{-1}) were used as the polar and dispersive liquids, respectively. As illustrated in Figure 2, as the PFDA content in the resist

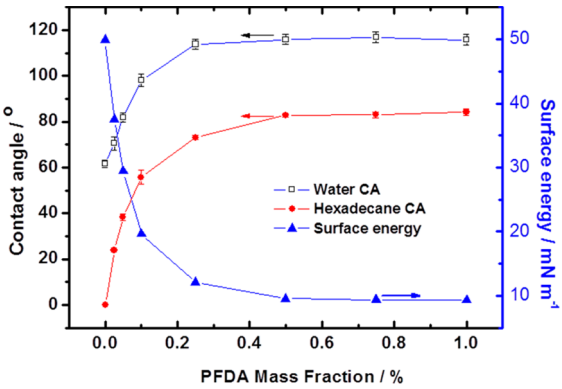

Figure 2. Water (open square) and hexadecane (solid circle) contact angles on a flat resist film as well as surface energy of the resist (solid triangle) as a function of PFDA mass fraction.

increased, the surfaces became more hydrophobic and less oleophilic. Specifically, at a PFDA mass fraction of around 0.1 wt %, the surface changed from hydrophilic to hydrophobic. With a further increase of the PFDA content, the contact angle of water and hexadecane increased and reached a plateau of around 116° and 83°, respectively. The estimated surface energy decreased from 49.9 mN m^{-1} to less than 10 mN m^{-1} as the concentration of PFDA was increased. The surface energy plateau value (10 mN m^{-1}) at PFDA concentrations greater than 0.5 wt % is comparable to the value of about 6.1 mN m^{-1} of pure poly(perfluorodecyl acrylate), which is among the lowest values for fluoro-containing polymers.[29]

The water and hexadecane contact angles as well as the estimated surface energy indicate that even a very low amount of PFDA (~0.50 wt %) can significantly enhance the hydrophobicity of the resist coating. It is well-known that polymer chains with low free surface energy, such as perfluorinated alkyl segments, tend to migrate to the polymer−air interface due to favorable thermodynamic interaction forces between low surface energy moieties and air.[30,31] The enrichment of fluoroalkyl chains on the surface was confirmed by surface elemental composition analysis using XPS (Figure S1). With the addition of PFDA, an intense fluorine peak appears in the XPS spectra. The fluorine elemental percentage increases with the PFDA fraction and reaches as high as 50%, which is substantially higher than the overall proportion of fluorine in the resist that consists of only 1.0 wt % of PFDA. The fluorine content in the top layer ~1.5 nm from the surface (15° takeoff angle) is much higher than that in the top ~4 nm layer (75° takeoff angle). XPS analysis indicates a substantial surface enrichment of low surface energy fragments, which is consistent with the change in resist surface energy. Therefore, the low surface energy resist with PFDA content higher than 0.50 wt % is suitable for R2R NIL fabrication of SHS.

Scheme 1a,b illustrates the R2R NIL process, including resist coating, imprinting, and curing. A 70 wt % solution of resist

Scheme 1. (a) Schematics of R2R UV NIL and Lubricant Coating Process and Cartoons of (b) R2R UV NIL Process and (c) R2R Lubricant Coating

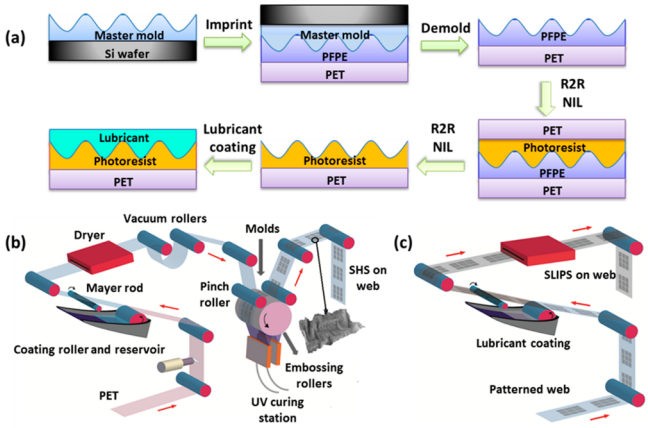

dissolved in propylene glycol monomethyl ether acetate (PGMEA) was coated on the PET substrate using a coating roller, and excess resist solution was removed using a Mayer rod (No. 2.5) to give a ~ 5 μm thick resist coating. The remaining solvent in the resist was removed using a forced air drying station as the web moved forward.

Master molds containing the requisite structures for R2R NIL were fabricated by inducing wrinkles on prepatterned poly(2-hydroxyethyl methacrylate) (PHEMA) films, as shown in Figure S2a. The complete description of the wrinkling process can be found in our previous publication.[24] As shown in Figure S2b,c, hierarchical structures with a combination of nanopillars on microwrinkles were prepared on silicon wafers. PFPE hybrid daughter molds were replicated from the wrinkled master molds, attached to a rubber cushion layer with double-sided adhesive tape, and wrapped around the embossing roller.[25] As the web was fed into the embossing roller, the two vacuum rollers applied tension against the photoresist-coated web and the molds. The tension forced the resist into the mold patterns; the resist was then rapidly cured using a UV light source (Omnicure 1000, EXFO with an intensity of 2 W cm^{-2}). The web with a cured patterned photoresist was continuously separated from the embossing roller molds and rewound on a take-up roll as the web moved forward. The web speed was kept at 10 in. min^{-1} for both coating and imprinting and can be further increased by using a higher intensity UV source.

Successful patterning was accomplished, and Figure 3a shows a sample web that is a few meters in length produced by the imprint process. Figure 3b displays a piece of fabricated pattern on the flexible PET substrate. SEM and AFM micrographs depict the surface structures of the imprinted webs (Figures 2c−f). Large wrinkled structures on the scale of tens of micrometers are present randomly throughout the film (Figure 3c), and regularly arrayed square nanopillars (700 nm size, 1 μm periodicity, and 750 nm height) rest on the wrinkled waves, giving rise to complex, hierarchical structures (Figures 3d,e). The inset AFM micrograph (Figures 3f) reveals the expanded and contracted area of the pillar patterns, corresponding to the stretched peak area and compressed valley area of the wrinkled structure, respectively. Figure S2 depicts SEM micrographs of

DOI: 10.1021/acsami.5b04957
ACS Appl. Mater. Interfaces 2015, 7, 23439−23444

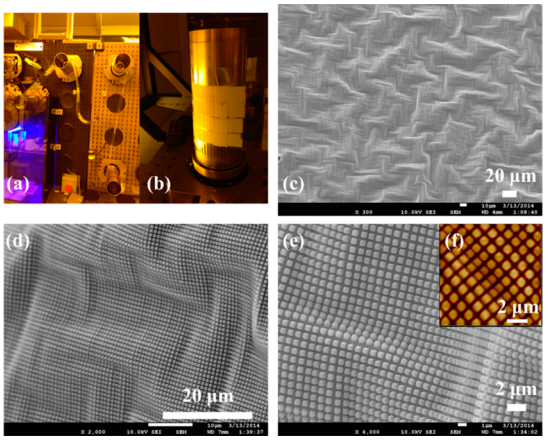

Figure 3. R2R NIL fabricated patterns: (a, b) photographs of nanoimprinted web in a R2R process, (c–e) SEM images of patterned surfaces, and (f) AFM images of patterned surfaces. Scale bars: (c, d), 20 μm; (e, f), 2 μm.

hierarchical structures on both the master mold and the imprinted substrate. The exact transfer of both the wrinkling structures and the pillar patterns from the master mold to the PET web demonstrates the excellent replication fidelity of R2R NIL.

The patterned surface exhibits superhydrophobicity without the need of any further chemical treatments. A spherical droplet of water (Figure 4a) on the patterned web surface can slide

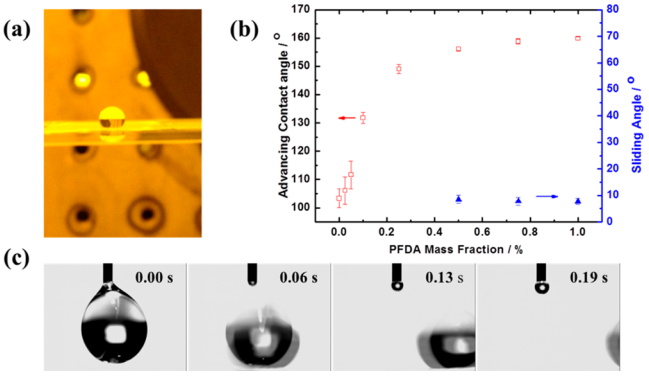

Figure 4. (a) Water droplet rested on a R2R imprinted web. (b) Advancing water contact angle (open square) and sliding angle (solid triangle) as a function of PFDA mass fraction; at PFDA concentrations less than 0.5 wt %, the water droplet (6 μL) adhered tightly on the surface and did not slide even at a titling angle of 90°; therefore, no sliding angle was reported. (c) Sliding of a water droplet from SHS upon tilting.

away easily when the web is tilted. As compared with a flat hydrophobic resist with CA of 116°, the wrinkle patterned surface has a much higher CA of around 160°. This enhancement of hydrophobicity is attributed to the hierarchical roughness (pillars resting on sinusoidal wrinkles).[32] The effect of PFDA concentration in the resist is evaluated by plotting the advancing water contact angle and sliding angle on the imprinted patterns as a function of PFDA content (Figure 4b). As expected, the water contact angle increases from around 100° without PFDA to near 160° with PFDA content higher than 0.5 wt %. The increase in the contact angle is consistent with the decrease in the resist's surface energy, a direct result of increasing the PFDA content. At PFDA concentrations below 0.5 wt %, the water droplet (6 μL) adhered to the patterned surfaces and did not move even at a titling angle of 90° (hence, no data for this is entered into Figure 4b). At PFDA content higher than 0.5 wt %, the wrinkled surface becomes superhydrophobic and the water droplet can readily slide away at a tilting angle of less than 10° (Figure 4b,c). The change in the advancing water contact angle and sliding angle revealed that increasing the PFDA concentration correlated with a transition in the wetting condition: from a wetting condition where water is fully impaled (Wenzel state) to the nonwetting Cassie–Baxter state with enhanced hydrophobicity.

SLIPS were achieved by coating the imprinted PET substrate with Krytox perfluoropolyether lubricant using a Mayer rod coating station (Scheme 1c). SLIPS showed enhanced optical transparency as compared with that of SHS (Figure S3), which is attributed to the decreased light scattering because of the liquid lubricant coating.[8] The stability of SLIPS was evaluated by observing the change in CA during the incubation of SLIPS under aqueous conditions. After a 5 day incubation, the water CA of the SLIPS substrate stabilized around 114° and the contact angle hysteresis (CAH) increased slightly but still remained low (<5°, Figure S4), indicating that the SLIPS were very stable upon incubation.

The wetting behavior of SHS and SLIPS was compared using standard liquids: hexadecane (γ = 27.5 mN m^{-1}), ethylene glycol (γ = 44.8 mN m^{-1}), glycerol (γ = 64.0 mN m^{-1}), and water (γ = 72.8 mN m^{-1}).[33] The results are plotted in Figure 5a

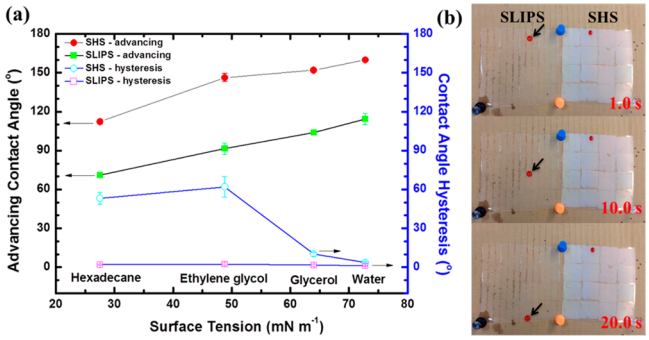

Figure 5. (a) Advancing water contact angle (solid) and contact angle hysteresis (open) on SHS (circle) and SLIPS (square) as a function of the testing liquid's surface tension. (b) Mobility of a hexadecane droplet (stained with oil red O) on SLIPS and SHS with a tilting angle of 20°.

and show that the contact angle of both surfaces increased with increasing liquid surface tension. As for the SHS samples, CAHs were low (<10°) for the high surface tension liquids, water and glycerol, whereas in the case of low surface tension liquids, ethylene glycol and hexadecane, the CAHs were much higher (>50°). Accordingly, the droplets of water and glycerol could readily slide away from SHS at a low tilting angle (<10°), whereas ethylene glycol and hexadecane droplets were pinned tightly onto the SHS even at a tilting angle of 90°. In comparison, SLIPS exhibited extremely low CAHs (<5°) for both high and low surface energy liquids. All of the liquids tested easily slipped away from the surface at a low tilting angle. Figure 5b shows the mobility of hexadecane droplets (stained with oil red O) on 8 × 8 cm^2 SLIPS and SHS samples tilted at 20°. Hexadecane quickly slid away from SLIPS, whereas it was firmly arrested on SHS. A comparison of the wetting behaviors of SHS and SLIPS suggests that the SLIPS has a superior self-

DOI: 10.1021/acsami.5b04957
ACS Appl. Mater. Interfaces 2015, 7, 23439–23444

cleaning capability for low surface tension liquid contaminations.

To explore the potential biomimetic applications of the flexible, large area SHS and SLIPS manufactured by R2R nanoimprinting, the antibiofouling properties were investigated by challenging the surfaces with *E. coli*. The samples were incubated in bacteria solution for 2 h, and the attachment of *E. coli* on the sample surface was quantified using confocal laser scanning microscopy (CLSM). As shown in Figure 6, flat resist

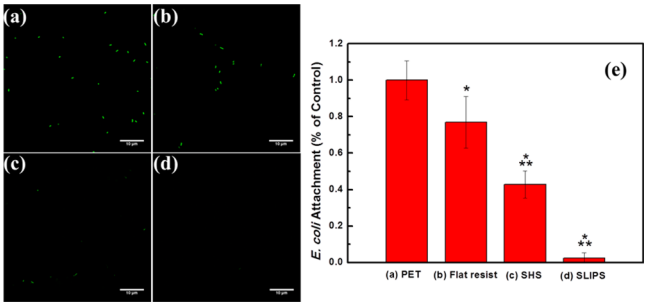

Figure 6. Fluorescence micrographs of *E. coli* attached to (a) PET, (b) flat resist, (c) SHS, and (d) SLIPS. (e) Normalized *E. coli* attachment on PET, flat resist, SHS, and SLIPS. All values are normalized to the coverage of *E. coli* on the PET control. Asterisks (*) and (**) denote statistical significance with a p value of 0.01 in reference to the PET control and the flat resist, respectively. Scale bar: 10 μm.

films exhibited ~20% less bacterial attachment than a bare PET substrate. The SHS displayed substantially lower adhesion of *E. coli* than the PET substrate, ~60% less bacteria. The outstanding antibiofouling property of SHS is comparable to the surfaces described in the work of Freschauf et al.[34] and Rahmawan et al.,[35] where *E. coli* and calf pulmonary artery endothelial cells, respectively, poorly adhered to their superhydrophobic hierarchically wrinkled patterns. The superhydrophobic nature of the SHS along with its favorable surface chemistry and topography caused the SHS to resist microbial attachment.[34] By coating a layer of lubricant on SHS and creating a SLIPS surface, bacterial adhesion was reduced by 98% versus the PET control surface. To exclude the influence of the potential toxicity of the lubricant on the low adhesion of bacteria on SLIPS, the cytotoxicity of Krytox was assessed through standard live/dead staining of bacteria in solution.[36] *E. coli* was incubated in growth media (M9 minimal media) containing the lubricant (2.5 and 5%) for 2 h at 37 °C. Viability of *E. coli* was >95% under the tested conditions (Figure S5), indicating that under these conditions there is no evidence of Krytox cytotoxicity.

Figure 6d illustrates the low adhesion of *E. coli* on SLIPS. There are two reasons for this low adhesion. First, because the *E. coli* solution was not miscible with the lubricant, the bacteria could not penetrate through the lubricant layer into contact with the solid surface. Second, bacteria cannot anchor onto a lubricant surface. Therefore, any bacteria in contact with SLIPS can be easily released by any small perturbation or rinsing, contributing to the excellent antibiofouling function of SLIPS.[13]

CONCLUSIONS

We have described the fabrication and advanced function of biomimetic superhydrophobic surfaces (SHS) and slippery lubricant-infused porous surfaces (SLIPS). Our novel contribution includes the ability to accomplish this rapidly over large areas using roll-to-roll nanoimprint lithography. Flexible roll-to-roll molds are replicated from hierarchically wrinkled patterns and imprinted to a hydrophobic photoresist through a roll-to-roll UV nanoimprinting process. The imprinted patterns on flexible substrates exhibit superhydrophobicity with a water contact angle around 160° without any further surface chemical modification. By coating the patterned surface with a layer of lubricant, SLIPS are fabricated with outstanding repellence to various liquids. This is the first successful attempt to scale up the fabrication of SHS and SLIPS using a roll-to-roll nanoimprint lithography fabrication technique. We also report new patternable thiol−ene based photopolymers. These are hydrophobic, fast-curing polymers optimized for use in roll-to-roll UV nanoimprint lithography.

Both SHS and SLIPS show good antibiofouling properties, with 60 and 98% reductions in *E. coli* adhesion, respectively, as compared with a PET control. The R2R NIL process enables a cost-efficient way to produce SHS and SLIPS with excellent self-cleaning and antibiofouling properties on a large scale, providing great potential to realize the practical applications of such biomimetic surfaces.

ASSOCIATED CONTENT

Supporting Information

The Supporting Information is available free of charge on the ACS Publications website at DOI: 10.1021/acsami.5b04957.

XPS spectra, schematics of the formation of hierarchical wrinkle, SEM images of hierarchically wrinkled structures on both master molds and imprinted PET, image of optical transparency enhancement of SLIPS as compared with SHS, images of advancing water contact angles and contact angle hysteresis of SLIPS as a function of incubation time, and assessment of the cytotoxicity of the lubricant (PDF).

AUTHOR INFORMATION

Corresponding Author

*E-mail: krcarter@polysci.umass.edu.

Notes

The authors declare no competing financial interest.

ACKNOWLEDGMENTS

This research was kindly supported by the NSF Material Research Science and Engineering Center on Polymers at UMass (MRSEC) (DMR-0213695), the UMass Center for Hierarchical Manufacturing (CHM), a NSF Nanoscale Science and Engineering Center (CMMI-1025020), and a grant from the Panasonic Boston Laboratory. This investigation was supported by National Research Service Award T32 GM008515 from the National Institutes of Health.

REFERENCES

(1) Amigoni, S.; de Givenchy, E. T.; Dufay, M.; Guittard, F. Covalent Layer-by-Layer Assembled Superhydrophobic Organic-Inorganic Hybrid Films. *Langmuir* **2009**, *25*, 11073−11077.

(2) Kato, S.; Sato, A. Micro/Nanotextured Polymer Coatings Fabricated by Uv Curing-Induced Phase Separation: Creation of Superhydrophobic Surfaces. *J. Mater. Chem.* **2012**, *22*, 8613−8621.

(3) Ding, X. F.; Zhou, S. X.; Gu, G. X.; Wu, L. M. A Facile and Large-Area Fabrication Method of Superhydrophobic Self-Cleaning Fluorinated Polysiloxane/Tio2 Nanocomposite Coatings with Long-Term Durability. *J. Mater. Chem.* **2011**, *21*, 6161−6164.

DOI: 10.1021/acsami.5b04957
ACS Appl. Mater. Interfaces 2015, 7, 23439−23444

(4) Wu, L. Y. L.; Shao, Q.; Wang, X. C.; Zheng, H. Y.; Wong, C. C. Hierarchical Structured Sol-Gel Coating by Laser Textured Template Imprinting for Surface Superhydrophobicity. *Soft Matter* **2012**, *8*, 6232−6238.
(5) Hardman, S. J.; Muhamad-Sarih, N.; Riggs, H. J.; Thompson, R. L.; Rigby, J.; Bergius, W. N. A.; Hutchings, L. R. Electrospinning Superhydrophobic Fibers Using Surface Segregating End-Functionalized Polymer Additives. *Macromolecules* **2011**, *44*, 6461−6470.
(6) Dai, S. X.; Zhang, D. B.; Shi, Q.; Han, X.; Wang, S. J.; Du, Z. L. Biomimetic Fabrication and Tunable Wetting Properties of Three-Dimensional Hierarchical Zno Structures by Combining Soft Lithography Templated with Lotus Leaf and Hydrothermal Treatments. *CrystEngComm* **2013**, *15*, 5417−5424.
(7) Teisala, H.; Tuominen, M.; Aromaa, M.; Makela, J. M.; Stepien, M.; Saarinen, J. J.; Toivakka, M.; Kuusipalo, J. Development of Superhydrophobic Coating on Paperboard Surface Using the Liquid Flame Spray. *Surf. Coat. Technol.* **2010**, *205*, 436−445.
(8) Wong, T. S.; Kang, S. H.; Tang, S. K. Y.; Smythe, E. J.; Hatton, B. D.; Grinthal, A.; Aizenberg, J. Bioinspired Self-Repairing Slippery Surfaces with Pressure-Stable Omniphobicity. *Nature* **2011**, *477*, 443−447.
(9) Li, J. S.; Kleintschek, T.; Rieder, A.; Cheng, Y.; Baumbach, T.; Obst, U.; Schwartz, T.; Levkin, P. A. Hydrophobic Liquid-Infused Porous Polymer Surfaces for Antibacterial Applications. *ACS Appl. Mater. Interfaces* **2013**, *5*, 6704−6711.
(10) Xiao, L. L.; Li, J. S.; Mieszkin, S.; Di Fino, A.; Clare, A. S.; Callow, M. E.; Callow, J. A.; Grunze, M.; Rosenhahn, A.; Levkin, P. A. Slippery Liquid-Infused Porous Surfaces Showing Marine Antibiofouling Properties. *ACS Appl. Mater. Interfaces* **2013**, *5*, 10074−10080.
(11) Kim, P.; Wong, T. S.; Alvarenga, J.; Kreder, M. J.; Adorno-Martinez, W. E.; Aizenberg, J. Liquid-Infused Nanostructured Surfaces with Extreme Anti-Ice and Anti-Frost Performance. *ACS Nano* **2012**, *6*, 6569−6577.
(12) Chen, J.; Dou, R. M.; Cui, D. P.; Zhang, Q. L.; Zhang, Y. F.; Xu, F. J.; Zhou, X.; Wang, J. J.; Song, Y. L.; Jiang, L. Robust Prototypical Anti-Icing Coatings with a Self-Lubricating Liquid Water Layer between Ice and Substrate. *ACS Appl. Mater. Interfaces* **2013**, *5*, 4026−4030.
(13) Epstein, A. K.; Wong, T. S.; Belisle, R. A.; Boggs, E. M.; Aizenberg, J. Liquid-Infused Structured Surfaces with Exceptional Anti-Biofouling Performance. *Proc. Natl. Acad. Sci. U. S. A.* **2012**, *109*, 13182−13187.
(14) Anand, S.; Paxson, A. T.; Dhiman, R.; Smith, J. D.; Varanasi, K. K. Enhanced Condensation on Lubricant-Impregnated Nanotextured Surfaces. *ACS Nano* **2012**, *6*, 10122−10129.
(15) Zhang, X.; Shi, F.; Niu, J.; Jiang, Y. G.; Wang, Z. Q. Superhydrophobic Surfaces: From Structural Control to Functional Application. *J. Mater. Chem.* **2008**, *18*, 621−633.
(16) Tian, Y.; Su, B.; Jiang, L. Interfacial Material System Exhibiting Superwettability. *Adv. Mater.* **2014**, *26*, 6872−6897.
(17) Cui, Y. H.; Paxson, A. T.; Smyth, K. M.; Varanasi, K. K. Hierarchical Polymeric Textures Via Solvent-Induced Phase Transformation: A Single-Step Production of Large-Area Superhydrophobic Surfaces. *Colloids Surf., A* **2012**, *394*, 8−13.
(18) Xue, C. H.; Jia, S. T.; Zhang, J.; Ma, J. Z. Large-Area Fabrication of Superhydrophobic Surfaces for Practical Applications: An Overview. *Sci. Technol. Adv. Mater.* **2010**, *11*, 033002.
(19) Tan, H.; Gilbertson, A.; Chou, S. Y. Roller Nanoimprint Lithography. *J. Vac. Sci. Technol., B: Microelectron. Process. Phenom.* **1998**, *16*, 3926−3928.
(20) Ahn, S. H.; Guo, L. J. Large-Area Roll-to-Roll and Roll-to-Plate Nanoimprint Lithography: A Step toward High-Throughput Application of Continuous Nanoimprinting. *ACS Nano* **2009**, *3*, 2304−2310.
(21) Ahn, S. H.; Guo, L. J. High-Speed Roll-to-Roll Nanoimprint Lithography on Flexible Plastic Substrates. *Adv. Mater.* **2008**, *20*, 2044−2049.
(22) Sondergaard, R. R.; Hosel, M.; Krebs, F. C. Roll-to-Roll Fabrication of Large Area Functional Organic Materials. *J. Polym. Sci., Part B: Polym. Phys.* **2013**, *51*, 16−34.
(23) Li, Y. Y.; Peterson, J. J.; Jhaveri, S. B.; Carter, K. R. Patterned Polymer Films Via Reactive Silane Infusion-Induced Wrinkling. *Langmuir* **2013**, *29*, 4632−4639.
(24) Li, Y. Y.; Dai, S. X.; John, J.; Carter, K. R. Superhydrophobic Surfaces from Hierarchically Structured Wrinkled Polymers. *ACS Appl. Mater. Interfaces* **2013**, *5*, 11066−11073.
(25) John, J.; Tang, Y. Y.; Rothstein, J. P.; Watkins, J. J.; Carter, K. R. Large-Area, Continuous Roll-to-Roll Nanoimprinting with Pfpe Composite Molds. *Nanotechnology* **2013**, *24*, 505307.
(26) Hoyle, C. E.; Lee, T. Y.; Roper, T. Thiol-Enes: Chemistry of the Past with Promise for the Future. *J. Polym. Sci., Part A: Polym. Chem.* **2004**, *42*, 5301−5338.
(27) Khire, V. S.; Yi, Y.; Clark, N. A.; Bowman, C. N. Formation and Surface Modification of Nanopatterned Thiol-Ene Substrates Using Step and Flash Imprint Lithography. *Adv. Mater.* **2008**, *20*, 3308−3313.
(28) Owens, D. K.; Wendt, R. Estimation of the Surface Free Energy of Polymers. *J. Appl. Polym. Sci.* **1969**, *13*, 1741−1747.
(29) Tsibouklis, J.; Nevell, T. G. Ultra-Low Surface Energy Polymers: The Molecular Design Requirements. *Adv. Mater.* **2003**, *15*, 647−650.
(30) Schnurer, A. U.; Holcomb, N. R.; Gard, G. L.; Castner, D. G.; Grainger, D. W. Photopolymerized Epoxide Copolymer Thin Films with Surfaces Highly Enriched with Sulfonyl Fluoride Groups. *Chem. Mater.* **1996**, *8*, 1475−1481.
(31) Sun, F.; Castner, D. G.; Mao, G.; Wang, W.; McKeown, P.; Grainger, D. W. Spontaneous Polymer Thin Film Assembly and Organization Using Mutually Immiscible Side Chains. *J. Am. Chem. Soc.* **1996**, *118*, 1856−1866.
(32) Hancock, M. J.; Sekeroglu, K.; Demirel, M. C. Bioinspired Directional Surfaces for Adhesion, Wetting, and Transport. *Adv. Funct. Mater.* **2012**, *22*, 2223−2234.
(33) Wu, S. *Polymer Interface and Adhesion*; Marcel Dekker, Inc.: New York, 1982; p 151.
(34) Freschauf, L. R.; McLane, J.; Sharma, H.; Khine, M. Shrink-Induced Superhydrophobic and Antibacterial Surfaces in Consumer Plastics. *PLoS One* **2012**, *7*, e40987.
(35) Rahmawan, Y.; Jang, K. J.; Moon, M. W.; Lee, K. R.; Suh, K. Y. Anti-Biofouling Coating by Wrinkled, Dual-Roughness Structures of Diamond-Like Carbon (Dlc). *BioChip J.* **2009**, *3*, 143−150.
(36) Lehtinen, J.; Nuutila, J.; Lilius, E.-M. Green Fluorescent Protein-Propidium Iodide (Gfp-Pi) Based Assay for Flow Cytometric Measurement of Bacterial Viability. *Cytometry* **2004**, *60A*, 165−172.

DOI: 10.1021/acsami.5b04957
ACS Appl. Mater. Interfaces 2015, 7, 23439−23444